Adaptive optical fluorescence microscopy

Na Ji

The past quarter century has witnessed rapid developments of fluorescence microscopy techniques that enable structural and functional imaging of biological specimens at unprecedented depth and resolution. The performance of these methods in multicellular organisms, however, is degraded by sample-induced optical aberrations. Here I review recent work on incorporating adaptive optics, a technology originally applied in astronomical telescopes to combat atmospheric aberrations, to improve image quality of fluorescence microscopy for biological imaging.

As a species, we have long relied on optical imaging to explore nature. With our eyes, we monitor our interactions with the outside world and, from images formed on our retina, interpret the underlying principles and rules of nature. The invention of the telescope and microscope allowed us to transcend the limits of our senses. Visualizing structures too distant, dim, or minute for bare eyes to see has vastly expanded our knowledge[1].

The history of telescope and microscope development has been dominated by the quest for a perfect imaging instrument. Diffraction-limited microscopes, free from optical nonidealities and with resolution limited solely by the wave nature of light, were routinely manufactured in the nineteenth century. The past 20 years have witnessed intense research efforts on super-resolution microscopy[2], in which the limitation on microscopic resolution posed by diffraction has been surpassed, and molecules tens of nanometers apart can be resolved in cultured cells or ultrathin sections, as well as research efforts on methods for imaging structure and function within living organisms[3,4].

The effect of optical aberrations

However, nature intervenes when one's ambition goes beyond imaging ultrathin or optically ideal samples. Whether we would like to image synapses deep inside a mouse brain using a microscope or distant stars using a telescope, we must contend with optical aberrations introduced to the image-forming light waves by the sample itself.

Optical aberrations arise in complex samples because imaging instruments are designed to achieve optimal performance in samples with specific optical properties. For example, water-dipping microscope objectives focus light into a diffraction-limited spot in water (**Fig. 1a**). If the sample has a different refractive index from that of water, it changes the directions and phases of the light rays and distorts the wavefront of the light from the ideal spherical form (**Fig. 1b**). This deviation in phase or optical path length from the ideal wavefront, or optical aberration, prevents diffraction-limited imaging[5–7].

Optical aberrations affect image quality in both astronomy and microscopy. Before the light from a distant star reaches a telescope on the Earth's surface, it has to traverse the atmosphere, where air masses of varying refractive indices distort its wavefront and lead to dim and fuzzy images of the star (**Fig. 1c**). In live biological samples, light travels through a heterogeneous mixture of components of the sample (e.g., water, proteins, nuclear acids, polysaccharides, lipids), which have refractive indices different from that of the objective immersion medium. As a result, in a widefield microscope such as a light-sheet microscope, where the fluorescence emitted inside a specimen propagates through the specimen before forming an image on a camera, the fluorescence wavefront is often degraded by the sample (**Fig. 1d**). For point-scanning microscopes such as confocal or two-photon microscopes, where optimal imaging performance requires the tightest excitation focus, aberrations accumulated by the excitation light on its way to the focal plane blur and dim its focus, leading to degradations in resolution and contrast (**Fig. 1e**). In addition to sample-induced aberrations, microscopes themselves may also contain system aberrations caused by imperfections in optics or alignment, which further degrade image quality.

Janelia Research Campus, Howard Hughes Medical Institute, Ashburn, Virginia, USA. Correspondence should be addressed to N.J. (jin@janelia.hhmi.org).

RECEIVED 11 OCTOBER 2016; ACCEPTED 6 FEBRUARY 2017; PUBLISHED ONLINE 31 MARCH 2017; DOI:10.1038/NMETH.4218

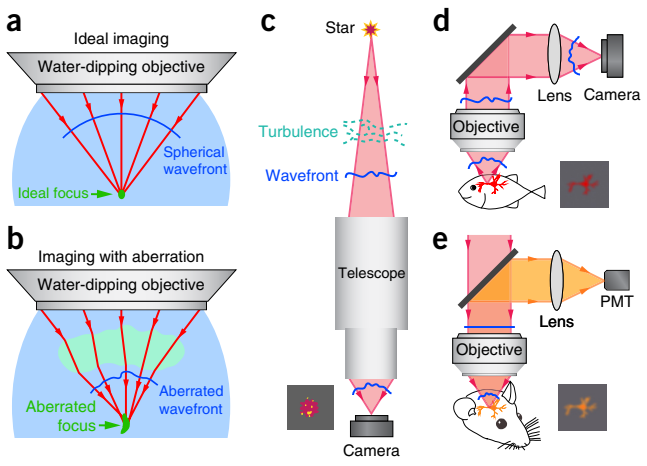

Figure 1 | Aberrations deteriorate image quality. (a) An ideal focus formed by a water-dipping microscope objective. (b) Refractive index mismatches from the water distort wavefront and lead to an aberrated focus. (c) A star's wavefront (blue lines) is distorted by the atmosphere, resulting in an aberrated image on a telescope (inset). Wavefronts of (**d**) fluorescence in a widefield microscope and (**e**) the excitation light in a point-scanning microscope are distorted by the sample, leading to images of reduced contrast and brightness (insets). PMT, photomultiplier tube.

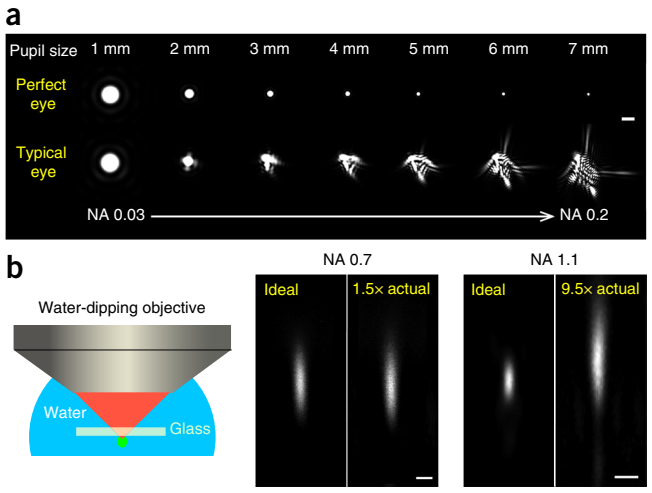

Figure 2 | High-resolution image system is more susceptible to aberrations. (**a**) Lateral PSFs of human eye degrade with the increase of pupil size and NA[9]. Scale bar, 10 µm. (**b**) A no. 1.5 glass coverslip leads to more severe signal and resolution degradation for a 1.1-NA than a 0.7-NA water-dipping objective. Aberrated axial two-photon excitation PSFs measured from 0.2-µm beads are shown in comparison to the ideal PSF. Brightness increases by 1.5-fold and 9.5-fold as indicated. Scale bars, 1 µm.

It is straightforward to detect the presence of aberrations in a microscope. By placing an object approximating a point—for example, a fluorescent bead of subdiffraction dimension—inside or below a specimen and measuring its image in 3D with the microscope, one obtains the 3D point-spread function (PSF). If the microscope itself is diffraction limited, any deviation of the PSF from that of a perfect optical system[8] indicates the presence of specimen-induced aberrations. Such deviations are more easily detectable in the axial PSF, which becomes enlarged and distorted before the lateral PSF shows obvious deterioration. Lower order aberrations, such as spherical aberration, astigmatism, and coma, have characteristic diffraction patterns near the focus and can also be identified from the PSF.

Problems associated with aberrations cannot be solved by improving the system's resolving power. For many samples, instruments with higher numerical aperture (NA) can experience larger aberrations, an effect familiar to anyone who has had one's pupil dilated. An imperfect imaging system, our eye has intrinsic aberrations. A dilated pupil increases the NA and admits in more light, but it allows the inclusion of higher order aberrations to degrade image formation, leading to increasingly distorted PSFs[9] (**Fig. 2a**) and blurred vision (this is also the reason that near- or far-sighted eyes see better in bright light through constricted pupils). Without correcting for sample-induced aberrations, increasing the NA of the imaging system (using a higher NA microscope objective, for instance) may help with light collection, but it would shift the performance of the system further away from the ideal diffraction limit (**Fig. 2b**).

Active and adaptive optics in microscopy

Ideal imaging performance can be achieved in aberrating samples if the wavefront distortion is compensated for by actively controlling the wavefront(s) involved in image formation. Lenses have been used as spectacles to reduce the aberrations in human eyes since at least the thirteenth century, and correction collars were introduced to microscope objectives in 1835 to minimize image degradation by variations in coverglass thickness[10]. Routine corrections of complex optical aberrations with active and adaptive optics (AO), however, were only realized experimentally after the maturation of wavefront measurement and control technologies in the late twentieth century[11,12].

Originally proposed to correct for the wavefront distortion caused by the Earth's atmosphere in telescopes, AO is conceptually simple; if the aberration is known, be it sample induced or intrinsic to the optical system, a wavefront modulator can be employed to introduce a compensatory distortion and minimize the net aberration before image formation. The same concept applies to AO in microscopy, where the most common wavefront correction devices are deformable mirrors and liquid crystal spatial light modulators[13]. Once calibrated, these devices are straightforward to use and robust in their performance. The various implementations of AO schemes in microscopy differ in how the aberration is measured and, based on this measurement, may be classified into direct and indirect wavefront measurement systems.

Direct wavefront measurement

In direct wavefront measurement, aberration is measured directly from a received wavefront (**Fig. 3**). In a telescope, after traveling through the atmosphere, light from a natural star or an artificial one (generated, e.g., by shining a laser into the mesosphere) is gathered by the telescope, reflected off a deformable mirror, and directed to a wavefront sensor (**Fig. 3a**). The wavefront sensor determines the point-by-point phase of the received wavefront. This information is then used to direct the shape of the deformable mirror to minimize aberration and achieve optimal resolution. With AO, Keck Observatory was able to resolve the stars near Sagittarius A*, the supermassive black hole in the center of the Milky Way (insets, **Fig. 3a**; UCLA Galactic Center Group, http://www.galacticcenter.astro.ucla.edu).

Similar optical geometries can be applied to microscopy. Unlike in telescopic studies of extraterrestrial objects, isolated,

self-luminous objects rarely occur naturally in biological specimens. Instead, a light-emitting source can be generated by fluorescence excitation or back scattering of the excitation light. The light emitted by such a 'guide star' (**Box 1**) accumulates aberrations while traversing the sample and instrument before reaching a wavefront sensor where its wavefront is measured.

To determine the phase profile of the wavefront, a sensor may interfere the wavefront with a reference wave or, more commonly, measure the local slope of the wavefront using the Shack–Hartmann (SH) scheme. In an SH sensor, a 2D array of lenses segments the wavefront and focuses light rays within individual segments onto a camera. From the displacements of the focus array relative to the displacement of an aberration-free wavefront (e.g., generated by a nonaberrating sample), the local slope of each wavefront segment is calculated (**Fig. 3b**) and the wavefront reconstructed. Such a direct wavefront sensing approach only works when there are sufficient ballistic, unscattered photons of the guide star reaching the wavefront sensor, because scattering leads to a loss of phase information as manifested in diffusive foci on the wavefront sensor (**Fig. 3c**). As a result, direct wavefront sensing can be applied to cultured cells and transparent tissues; and it can also be applied within the superficial depths of opaque samples such as the mouse brain (up to ~2 scattering lengths[14]). The first demonstration of adaptive optics for imaging biological samples employed direct wavefront sensing; aberration of human eyes was measured with light back reflected from the retina as the guide star and corrected to achieve high-resolution retinal imaging[15].

For widefield fluorescence microscopes where an extended volume is illuminated simultaneously, aberration correction is often only needed for the emitted fluorescence (**Figs. 1d** and **3d**). Azucena *et al.*[16] and Azucena *et al.*[17] injected fluorescent beads in *Drosophila* embryos and measured the aberration of their fluorescence after it passed through the embryo with an SH wavefront sensor in a widefield microscope. Using fluorescent beads incorporated into 3D multicellular tumor spheroids, Jorand *et al.*[18] corrected the spheroid-induced aberrations in the detection path of a selective-plane illumination microscope. In both examples, with a closed loop between a wavefront sensor and a deformable mirror, the detected wavefront error was minimized, resulting in improvements in image quality (insets, **Fig. 3d**).

For two-photon excitation fluorescence microscopes with pinhole-free nonimaging detectors (e.g., photomultiplier tubes), aberration correction is only needed for the excitation light (typically ultrashort laser pulses in the near-infrared range), because the quality of the excitation focus determines imaging performance (**Figs. 1e** and **3e**). In samples where direct wavefront sensing is applicable, the aberration of the excitation light that is back scattered from its focus can be directly measured. Rueckel *et al.*[19] used a coherence-gated wavefront sensing scheme where an ultrashort pulse with appropriate time delay was used as a coherence gate to select back-scattered excitation light that originated near the focus and measured its wavefront aberration via interference. Cha *et al.*[20] used a confocal pinhole to select excitation light reflected from the focal region and an SH sensor to measure its wavefront. In fluorescent samples, because two-photon excitation naturally produces a fluorescent signal confined in a compact focal volume, this signal can be used as the guide star. Given the low chromatic dispersion of biological

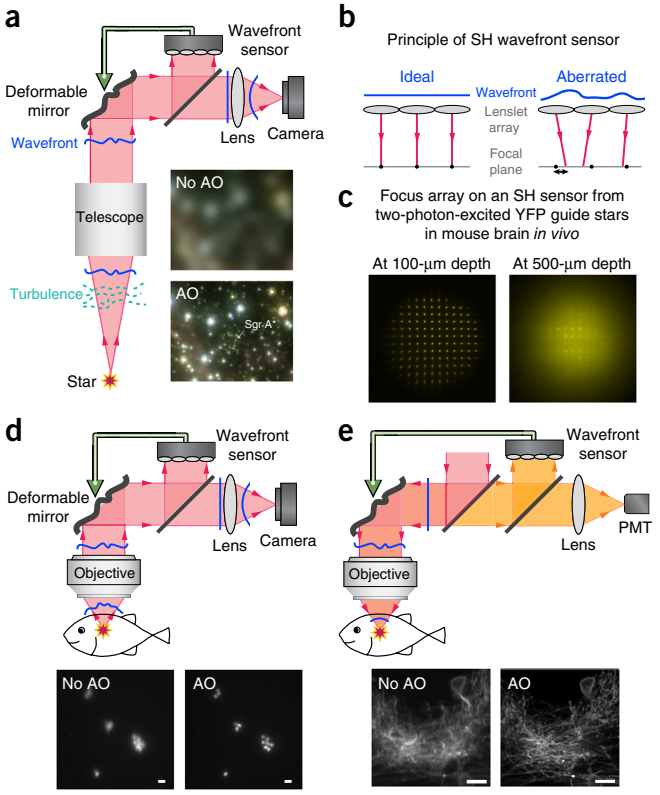

Figure 3 | Adaptive optics using direct wavefront sensing. (**a**) Distortion of wavefront (blue lines) is directly measured with a wavefront sensor and minimized by a wavefront modulator (e.g., a deformable mirror) to improve image quality for a telescope. Sgr A*, Sagittarius A*. (**b**) Principle of SH wavefront sensor. (**c**) Images on a SH sensor of two-photon-excited YFP guide stars at 100- and 500-µm depth inside a mouse brain *in vivo*. (**d**,**e**) Direct-wavefront-sensing-based adaptive optical widefield fluorescence microscope (**d**) and two-photon fluorescence microscope (**e**). Insets represent images of (**a**) stars near Sagittarius A*, (**d**) beads inside a *Drosophila* embryo[17], (**e**) neurons in zebrafish larval brain[22] obtained without and with AO correction. Scale bars, 2 µm (**d**) and 10 µm (**e**).

samples, specimen-induced aberrations of the excitation light can be approximated by the wavefront distortion experienced by the emitted fluorescence as it propagates out of the sample and is directly measured by an SH sensor. Such a nonlinear-excitation-generated guide star was used to improve the image quality of *Caenorhabditis elegans in vivo*[21]. When an averaged aberration over small sample volumes was measured, Wang *et al.*[22] achieved near-diffraction-limited imaging in large volumes (>240 µm per side) in zebrafish larval brains *in vivo* using rapid (~tens of milliseconds per wavefront) direct wavefront sensing of fluorescent guide stars in the visible wavelengths (insets, **Fig. 3e**). In more opaque tissues such as the mouse brain, we can extend the depth to which direct wavefront sensing is applicable by using guide stars of longer wavelengths. The reduced scattering of near-infrared fluorescence allowed us to extend direct wavefront sensing down to 700 µm inside the mouse brain and to resolve dendritic spines down to 760 µm *in vivo*[14].

For confocal fluorescence microscopy, aberration correction improves both the illumination by providing a tighter excitation focus and the detection by ensuring that the in-focus fluorescence passes through the confocal pinhole, which requires both the

BOX 1 VOCABULARY

Active and adaptive optics are methods in which the wavefront of an imaging system is controlled, sometimes in real time, to optimize image performance in the presence of optical aberrations.

Optical aberrations are of two classes—monochromatic and chromatic aberrations. Dispersion, or the variation of material refractive index with wavelength, causes chromatic aberration, where lights of different wavelengths follow distinct optical paths. Chromatic aberration is usually well corrected in modern imaging instruments, and typical biological samples have small dispersion; thus we only consider monochromatic aberrations here. Aberration of a wavefront is quantified as the difference in its phase or optical path length from the ideal (e.g., spherical or planar) form. Mathematically, it can be described as a summation of Zernike polynomials, a set of basis functions that are orthogonal within a circle (in this case, the objective back pupil). Low-order Zernike modes are related to the primary aberrations such as spherical aberration, coma, and astigmatism.

A **wavefront** is a 3D surface with constant optical path length and is always orthogonal to the corresponding light rays. A converging spherical wavefront leads to a diffraction-limited focus with all rays converging to the focal point.

A **guide star** is a 3D confined light source located inside the sample. The wavefront of the guide star accumulates aberrations while propagating out of the sample and is directly measured by a wavefront sensor. A guide star can be from either the excitation light generated by reflection or back scattering, or the fluorescence emission via one- or two-photon excitation.

Deformable mirrors are membrane mirrors whose surface can be actively controlled, and they are either continuous or segmented. They have high bandwidth (>1 KHz) and operate over large wavelength ranges, but they become expensive with increasing numbers of actuators (typical mirrors for adaptive optical microscopy have <100 actuators).

Liquid crystal spatial light modulators are devices made of typically 100,000s or even millions of liquid crystal cells that impose spatially varying modulation on the wavefront of the light. For AO applications, each cell imparts a phase delay. The large numbers of pixels allow correction of very high-order aberrations, but LC-SLMs operate within a narrower wavelength range (~100s nm) for a specific polarization, and they typically update at a much lower rate (~60 Hz).

excitation and the emission light to reflect off the deformable mirror. Using isolated fluorescent beads as fluorescent guide stars, Tao *et al.*[23] improved the signal and contrast of images of mouse brain tissue. Using endogenous fluorescence of the samples requires additional attention, especially for samples with high label density. The confocal pinhole size needs to be carefully selected so that it blocks out-of-focus fluorescence without excessively filtering out higher-order aberrations[24,25]. Using fluorescent proteins as guide stars, Tao *et al.*[24] demonstrated AO corrections for YFP-labeled dendritic spines in fixed mouse brain slices and GFP-labeled centrosomes in live *Drosophila* embryos[26]. Careful adjustment of confocal pinhole size is no longer necessary when two-photon excitation is used to generate a guide star. Using this approach, Wang *et al.*[22] improved confocal images of oligodendrocytes and neuronal nuclei in larval zebrafish brain as well as images of dendrites in mouse brain *in vivo*, where apposed membranes and organelles became resolvable after specimen-induced aberrations were corrected[14].

Indirect wavefront measurement

Unlike the direct approaches where a dedicated sensor is used to measure a wavefront directly, AO fluorescence microscopy methods using indirect approaches vary widely in terms of how the optimal corrective wavefront is reached.

One class of methods is based on physical principles similar to how an SH wavefront sensor measures aberration, but instead using the focusing process in a microscope. In this approach, the slope of each wavefront segment is directly calculated from the displacement of the corresponding light ray from the desired focus (**Fig. 4a**). By illuminating one pupil segment at a time and recording the resulting two-photon fluorescence image, we measured the displacement of the corresponding excitation light ray in the focal plane (**Fig. 4a**,**b**)[27], from which the wavefront aberration could be reconstructed with algorithms used for SH sensors or with phase-shift values measured experimentally[27,28]. This approach allowed us to recover diffraction-limited imaging performance at a depth of 450 µm in mouse cortex *in vivo*[29]. We have also used it to correct system aberrations for two-photon fluorescence microendoscopy[30,31] and Scrimgeour *et al.*[32] has applied it to widefield microscopy. This serial 'pupil segmentation' method measures each segment at low NA and therefore requires the structure used for aberration measurement to be sparsely labeled, just as an SH sensor works best with isolated point-like sources. However, once the aberration measurement has been taken on a sparsely labeled structure, the correction can improve images of densely labeled structures in the same sample.

Alternatively, the entire pupil can be illuminated to produce a tighter focus and high NA. Because an aberrated ray requires extra tilt to overlap and optimally interfere with the reference focus formed by the remaining rays, we monitored fluorescence signal variation while tilting a light ray, and we determined the slope of the corresponding wavefront segment via the displacement of signal maximum from center (i.e., zero applied tilt)[33]. To speed up this process, each ray can be modulated at a distinct frequency, allowing the slopes of multiple segments to be measured simultaneously[34]. Using this frequency-multiplexed approach, we measured and corrected the aberrations in densely labeled *C. elegans*, zebrafish, and mouse brains *in vivo* (**Fig. 4b**).

Phase retrieval and phase diversity approaches[35], originally developed in astronomical AO, have also been applied to optical microscopy. Hanser *et al.*[36,37] showed that phase retrieval algorithms can calculate the wavefront from images of subdiffraction sources

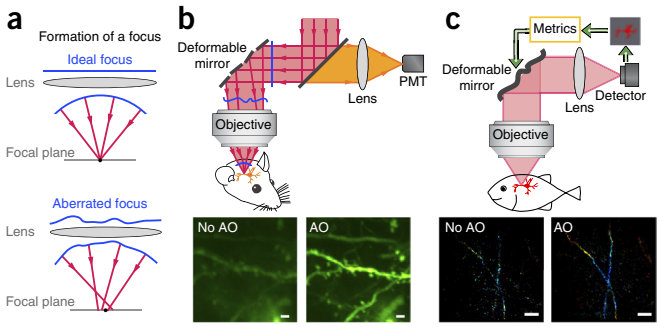

Figure 4 | Adaptive optical fluorescence microscopy with indirect wavefront sensing. (**a**) Formation of a focus without and with aberration. Black dots indicate focal positions in ideal aberration-free systems. (**b**) In a two-photon fluorescence microscope, the wavefront is separated into segments, and individual light rays representing each segment are measured and corrected to recover optimal imaging performance. Insets, dendritic spines in mouse brains imaged without and with AO correction[34]. (**c**) Metric-based optimization methods collect images with known wavefront distortions introduced, from which an optimal corrective wavefront is obtained. Insets, super-resolution single-molecule localization microscopic images of microtubules measured without and with AO correction[54]. Scale bars, 2 µm (**b**) and 1 µm (**c**).

at multiple defocus sections. Kner *et al.*[38] applied this approach to correcting microscope system aberration for a widefield microscope. The phase diversity method estimates both the aberration and the form and structure of the object from images taken with known phase distortions applied. Originally only applicable for 2D objects, phase diversity theory has been extended by Kner[39] to widefield imaging of 3D objects.

All the methods described above measure the aberrations directly. Aberration measurements without a conventional wavefront sensor may also be achieved by iteratively adjusting the wavefront until a certain image metric—such as brightness, sharpness, or contrast—is optimized (**Fig. 4c**). Image-brightness-based metrics work well for samples with constant and bright fluorescence; whereas metric functions based on spatial frequency, sharpness, or contrast are more suitable for systems with dimmer and/or fluctuating signals.

Genetic or hill-climbing algorithms have long been used to search for the optimal correction that maximizes image brightness[40–43]. Well suited for bright and nonbleaching signals, these algorithms have been used to correct the aberrations in optical systems[44] as well as to improve image quality in two-photon microscopy of *ex vivo* ocular tissue[45] and astrocytes in mouse brains *in vivo*[46].

Methods have also been developed to improve the metric-based optimization approaches by reducing the number of iterations needed to reach optimal correction[47]. Similar to phase diversity, these 'modal' approaches use a wavefront modulator such as a deformable mirror to introduce a known aberration. A quality metric of the collected image—based on brightness, contrast, sharpness or combinations thereof—is then calculated. Because the metric is (in certain cases) explicitly related to the amount of aberrations[48–50], the amplitude of each aberration mode introduced by the sample can be estimated by measuring the metrics when different amplitudes of the same aberration mode are applied. Compared with the genetic or hill-climbing methods, the modal approach substantially reduces the number of images that need to be taken. Using signal brightness as the metric, Booth *et al.*[48] demonstrated improvements in image quality of confocal microscopy in mouse intestine, and Débarre *et al.*[51] increased the brightness and contrast of two-photon fluorescence microscopy in mouse intestine and embryo. For widefield optical sectioning structured-illumination microscopy, Débarre *et al.*[50] used image sharpness as a metric and achieved better contrast and rejection of out-of-focus background in fluorescent mouse intestine and pollen grains. Using image contrast as a metric, Bourgenot *et al.*[52] improved images of zebrafish in a light-sheet microscope by correcting the aberrations introduced by glass or plastic pipettes.

Direct and indirect wavefront sensing methods differ substantially in their ease of implementation, speed of aberration measurement, and performance. As they require only a wavefront correction device, indirect sensing methods are simpler in hardware implementation and can be applied to opaque tissue. However, they are slower in measuring aberration, taking seconds to minutes, whereas direct wavefront sensing methods can reach a corrective wavefront within tens of milliseconds, but only in transparent or weakly scattering samples. Such high speed, however, requires sufficiently bright guide stars—for example, fluorescent fiducials or highly expressed fluorescence proteins. The requirement of both a wavefront sensor and modulator also increases the cost and complexity of the direct wavefront sensing methods.

Adaptive optics in super-resolution microscopy

With resolutions at tens of nanometers, the performance of super-resolution fluorescence microscopy is even more sensitive to aberration than are diffraction-limited systems, because an ideal PSF is usually required for super-resolution methods to function[53]. Because high-NA objectives are employed in these microscopes, aberrations from the instruments themselves can also become substantial and require AO correction.

In principle, once sample-induced aberrations are fully corrected in the regime of diffraction-limited microscopy, ideal imaging performance should also be attained in their super-resolution counterparts. Therefore, the AO methods reviewed above that can correct aberrations with high accuracy can be directly applied to super-resolution methods. Specifically, widefield AO methods can be applied to single-molecule localization microscopy (SMLM) as well as to structured illumination microscopy (SIM), whereas correction procedures for point-scanning microscopy can be applied to methods such as stimulated emission depletion (STED) microscopy.

For SMLM, aberrations reduce the brightness and localization accuracy of single-molecule fluorescence. Both direct[44] and indirect[54,55] sensing methods have been used for system aberration correction in SMLM. Genetic algorithms based on fiducial marker brightness[44] or single-molecule-frame spatial frequency[56] and an image-sharpness-based modal approach[54] have been applied to correct aberrations through fixed cells and *Drosophila* brain lobes, resulting in brighter single molecules, higher localization density, and greater precision (insets, **Fig. 4c**). In certain cases, SMLM benefits from simply knowing the aberrations in the system. Through acquiring 3D PSFs across the field of view by either phase retrieval and computation[57] or direct measurements[58], the axial positional distortions caused by system aberrations have been corrected in 3D SMLM systems.

AO has also been applied to SIM, where structured illumination patterns are used to down modulate high-frequency spatial information of the sample to within the diffraction limit and effectively double the spatial resolution. Aberrations in the fluorescent detection path reduce image brightness and, more importantly, cause artifacts during image reconstruction[59]. Thomas *et al.*[60] used phase retrieval to correct system aberration in an AO-SIM system and applied a modal approach to improve the images of fluorescent beads through a 35-µm-thick *C. elegans*.

To achieve super-resolution in STED microscopy, it is essential to have zero intensity in the center of the depletion focus. Aberrations that lead to a distorted depletion focus and nonzero central intensity degrade resolution and quench the desired fluorescence at the center[53]. AO was used to correct system aberration in the depletion beam by Auksorius *et al.*[61] and Lenz *et al.*[62] with a modal approach. We used the pupil-segmentation method to correct system aberrations in a two-photon microscope to recover the central zero intensity in the annular focus typically used for 2D STED[27]. Using two image metrics on brightness and sharpness, Gould *et al.*[63] corrected aberrations introduced by 25-µm-thick zebrafish retina sections and improved both the brightness and resolution of fluorescent beads underneath.

Practical considerations

There is no simple answer to the question of what the optimal AO method is for a particular sample–microscope combination, as it depends on the characteristics of the sample and the aberrations to be corrected as well as, practically, the available expertise and budget. However, some general conclusions can be reached. Comparing direct with indirect sensing methods, direct methods are faster in measuring aberration, whereas indirect methods are less complex to implement and can be applied to both transparent and scattering tissue. Given bright guide stars, direct methods may have higher accuracy in wavefront measurement, especially when compared with that of the iteration-based indirect sensing methods.

An important factor to consider when applying wavefront shaping to optical microscopy is the size of the isoplanatic patch, the area within which a single correction provides substantial improvement in image quality. For aberration correction in biological samples, isoplanatic patch size depends on sample morphology, refractive index heterogeneity, and wavefront sensing methods. Specimens with low surface curvature (e.g., the mouse brain) may have isoplanatic patches hundreds of microns in dimension[14,29,34], whereas in samples with high surface curvature (e.g., *C. elegans* or zebrafish larvae), a single aberration correction may only improve image quality in the vicinity of the aberration measurement location[22,34]. For transparent samples with small isoplanatic patches (i.e., brains of zebrafish larvae), direct wavefront sensing has been used to provide AO recovery at a 14-ms update rate for optimal image quality over hundreds of microns[22].

It has been demonstrated, for all the AO methods reviewed above, that aberration correction improves image quality in fluorescence microscopy. Because even partial correction of existing aberrations leads to brighter and sharper images, to determine how close to the diffraction-limited performance the microscope operates after AO correction, it is advisable, whenever possible, to measure and report the axial PSF (**Fig. 2b**) or images (because of their sensitivity to aberrations) with the corrected system.

In addition to AO methods for aberration correction, the past 10 years have also witnessed the rapid development of wavefront shaping methods that combat light scattering. On account of the highly spatially varying distribution of scatterers, these techniques arrive at wavefront corrections with very small (micron-sized) isoplanatic patches. These scattering control techniques have been reviewed recently[64–66] and are not discussed here.

Future directions

Though research efforts on AO microscopy have been largely focused on the most common modalities of single- or two-photon excitation fluorescence, similar approaches can improve the performance of optical microscopy in aberrating samples in general. Correcting aberrations is especially important for microscopy involving higher-order nonlinear optical processes, such as in three-photon excitation fluorescence[67] third harmonic generation[68].

Ultimately, the applications of AO to microscopy need to go beyond technical, proof-of-principle demonstrations. We need to make existing methods simple to use and robust in performance, as well as prove that AO can enable biological discoveries, which requires close collaborations between microscopists and biologists, as demonstrated recently[69].

With the rapid incorporation into both diffraction-limited and super-resolution microscopy, one envisions that adaptive optics will soon be an essential element for all high-resolution imaging deep in multicellular specimens.

ACKNOWLEDGMENTS

The author thanks A. Roorda and R. Turcotte for providing data in **Figure 2**. This work is supported by Howard Hughes Medical Institute.

COMPETING FINANCIAL INTERESTS

The author declares no competing financial interests.

1. Hooke, R. *Micrographia: or some physiological descriptions of minute bodies made by magnifying glasses with observations and inquiries thereupon* (Royal Society, 1665).
2. Schermelleh, L., Heintzmann, R. & Leonhardt, H. A guide to super-resolution fluorescence microscopy. *J. Cell Biol.* **190**, 165–175 (2010).
3. Power, R.M. & Huisken, J. A guide to light-sheet fluorescence microscopy for multiscale imaging. *Nat. Methods* **14**, 360–373 (2017).
4. Yang, W. & Yuste, R. *In vivo* imaging of neural activity. *Nat. Methods* **14**, 349–359 (2017).
5. Gibson, S.F. & Lanni, F. Experimental test of an analytical model of aberration in an oil-immersion objective lens used in three-dimensional light microscopy. *J. Opt. Soc. Am. A* **9**, 154–166 (1992).
6. Schwertner, M., Booth, M. & Wilson, T. Characterizing specimen induced aberrations for high NA adaptive optical microscopy. *Opt. Express* **12**, 6540–6552 (2004).
7. Török, P., Hewlett, S.J. & Varga, P. The role of specimen-induced spherical aberration in confocal microscopy. *J. Microsc.* **188**, 158–172 (1997).
8. Born, M. & Wolf, E. *Principles of Optics: Electromagnetic Theory of Propagation, Interference and Diffraction of Light* 7th edn. (Cambridge University Press, 1999).
9. Roorda,, A. in *Wavefront Customized Visual Correction: The Quest for SuperVision II* (eds. Macrae, S.M. *et al.*) Ch. 2 (Slack Inc., 2004).
10. Hartley, W.G. *The light microscope: its use and development* (Senecio Publishing Company, 1993).
11. Babcock, H.W. Adaptive optics revisited. *Science* **249**, 253–257 (1990).
12. Hardy, J.W. Active optics: a new technology for the control of light. In *Proc. IEEE* **66**, 651–697 (IEEE, 1978).

13. Booth, M.J. Adaptive optical microscopy: the ongoing quest for a perfect image. *Light Sci. Appl.* **3**, e165 (2014).
14. Wang, K. *et al.* Direct wavefront sensing for high-resolution *in vivo* imaging in scattering tissue. *Nat. Commun.* **6**, 7276 (2015).
15. Liang, J., Williams, D.R. & Miller, D.T. Supernormal vision and high-resolution retinal imaging through adaptive optics. *J. Opt. Soc. Am. A Opt. Image Sci. Vis.* **14**, 2884–2892 (1997).
16. Azucena, O. *et al.* Wavefront aberration measurements and corrections through thick tissue using fluorescent microsphere reference beacons. *Opt. Express* **18**, 17521–17532 (2010).
17. Azucena, O. *et al.* Adaptive optics wide-field microscopy using direct wavefront sensing. *Opt. Lett.* **36**, 825–827 (2011).
18. Jorand, R. *et al.* Deep and clear optical imaging of thick inhomogeneous samples. *PLoS One* **7**, e35795 (2012).
19. Rueckel, M., Mack-Bucher, J.A. & Denk, W. Adaptive wavefront correction in two-photon microscopy using coherence-gated wavefront sensing. *Proc. Natl. Acad. Sci. USA* **103**, 17137–17142 (2006).
20. Cha, J.W., Ballesta, J. & So, P.T. Shack-Hartmann wavefront-sensor-based adaptive optics system for multiphoton microscopy. *J. Biomed. Opt.* **15**, 046022 (2010).
21. Aviles-Espinosa, R. *et al.* Measurement and correction of *in vivo* sample aberrations employing a nonlinear guide-star in two-photon excited fluorescence microscopy. *Biomed. Opt. Express* **2**, 3135–3149 (2011).
22. Wang, K. *et al.* Rapid adaptive optical recovery of optimal resolution over large volumes. *Nat. Methods* **11**, 625–628 (2014).
23. Tao, X. *et al.* Adaptive optics confocal microscopy using direct wavefront sensing. *Opt. Lett.* **36**, 1062–1064 (2011).
24. Tao, X. *et al.* Adaptive optics microscopy with direct wavefront sensing using fluorescent protein guide stars. *Opt. Lett.* **36**, 3389–3391 (2011).
25. Rahman, S.A. & Booth, M.J. Direct wavefront sensing in adaptive optical microscopy using backscattered light. *Appl. Opt.* **52**, 5523–5532 (2013).
26. Tao, X. *et al.* Live imaging using adaptive optics with fluorescent protein guide-stars. *Opt. Express* **20**, 15969–15982 (2012).
27. Ji, N., Milkie, D.E. & Betzig, E. Adaptive optics via pupil segmentation for high-resolution imaging in biological tissues. *Nat. Methods* **7**, 141–147 (2010).
28. Liu, R., Milkie, D.E., Kerlin, A., MacLennan, B. & Ji, N. Direct phase measurement in zonal wavefront reconstruction using multidither coherent optical adaptive technique. *Opt. Express* **22**, 1619–1628 (2014).
29. Ji, N., Sato, T.R. & Betzig, E. Characterization and adaptive optical correction of aberrations during *in vivo* imaging in the mouse cortex. *Proc. Natl. Acad. Sci. USA* **109**, 22–27 (2012).
30. Wang, C. & Ji, N. Characterization and improvement of three-dimensional imaging performance of GRIN-lens-based two-photon fluorescence endomicroscopes with adaptive optics. *Opt. Express* **21**, 27142–27154 (2013).
31. Wang, C. & Ji, N. Pupil-segmentation-based adaptive optical correction of a high-numerical-aperture gradient refractive index lens for two-photon fluorescence endoscopy. *Opt. Lett.* **37**, 2001–2003 (2012).
32. Scrimgeour, J. & Curtis, J.E. Aberration correction in wide-field fluorescence microscopy by segmented-pupil image interferometry. *Opt. Express* **20**, 14534–14541 (2012).
33. Daniel, E., Betzig, E. & Ji, N. Pupil-segmentation-based adaptive optical microscopy with full-pupil illumination. *Opt. Lett.* **36**, 4206–4208 (2011).
34. Wang, C. *et al.* Multiplexed aberration measurement for deep tissue imaging *in vivo*. *Nat. Methods* **11**, 1037–1040 (2014).
35. Gonsalves, R.A. Perspectives on phase retrieval and phase diversity in astronomy. In *Proc. SPIE* Vol. 9148 (eds. Marchetti, E. *et al.*) 91482P (SPIE, 2014).
36. Hanser, B.M., Gustafsson, M.G.L., Agard, D.A. & Sedat, J.W. Phase retrieval for high-numerical-aperture optical systems. *Opt. Lett.* **28**, 801–803 (2003).
37. Hanser, B.M., Gustafsson, M.G.L., Agard, D.A. & Sedat, J.W. Phase-retrieved pupil functions in wide-field fluorescence microscopy. *J. Microsc.* **216**, 32–48 (2004).
38. Kner, P., Winoto, L., Agard, D.A. & Sedat, J.W. Closed loop adaptive optics for microscopy without a wavefront sensor. In *Proc. SPIE* Vol. 7570 (eds. Conchello, J.-A. *et al.*) 7570 06 (SPIE, 2010).
39. Kner, P. Phase diversity for three-dimensional imaging. *J. Opt. Soc. Am. A Opt. Image Sci. Vis.* **30**, 1980–1987 (2013).
40. Albert, O., Sherman, L., Mourou, G., Norris, T.B. & Vdovin, G. Smart microscope: an adaptive optics learning system for aberration correction in multiphoton confocal microscopy. *Opt. Lett.* **25**, 52–54 (2000).
41. Sherman, L., Ye, J.Y., Albert, O. & Norris, T.B. Adaptive correction of depth-induced aberrations in multiphoton scanning microscopy using a deformable mirror. *J. Microsc.* **206**, 65–71 (2002).
42. Marsh, P., Burns, D. & Girkin, J. Practical implementation of adaptive optics in multiphoton microscopy. *Opt. Express* **11**, 1123–1130 (2003).
43. Wright, A.J. *et al.* Exploration of the optimisation algorithms used in the implementation of adaptive optics in confocal and multiphoton microscopy. *Microsc. Res. Tech.* **67**, 36–44 (2005).
44. Izeddin, I. *et al.* PSF shaping using adaptive optics for three-dimensional single-molecule super-resolution imaging and tracking. *Opt. Express* **20**, 4957–4967 (2012).
45. Skorsetz, M., Artal, P. & Bueno, J.M. Performance evaluation of a sensorless adaptive optics multiphoton microscope. *J. Microsc.* **261**, 249–258 (2016).
46. Galwaduge, P.T., Kim, S.H., Grosberg, L.E. & Hillman, E.M.C. Simple wavefront correction framework for two-photon microscopy of *in vivo* brain. *Biomed. Opt. Express* **6**, 2997–3013 (2015).
47. Booth, M. Wave front sensor-less adaptive optics: a model-based approach using sphere packings. *Opt. Express* **14**, 1339–1352 (2006).
48. Booth, M.J., Neil, M.A.A., Juskaitis, R. & Wilson, T. Adaptive aberration correction in a confocal microscope. *Proc. Natl. Acad. Sci. USA* **99**, 5788–5792 (2002).
49. Booth, M.J. Wavefront sensorless adaptive optics for large aberrations. *Opt. Lett.* **32**, 5–7 (2007).
50. Débarre, D., Botcherby, E.J., Booth, M.J. & Wilson, T. Adaptive optics for structured illumination microscopy. *Opt. Express* **16**, 9290–9305 (2008).
51. Débarre, D. *et al.* Image-based adaptive optics for two-photon microscopy. *Opt. Lett.* **34**, 2495–2497 (2009).
52. Bourgenot, C., Saunter, C.D., Taylor, J.M., Girkin, J.M. & Love, G.D. 3D adaptive optics in a light sheet microscope. *Opt. Express* **20**, 13252–13261 (2012).
53. Booth, M., Andrade, D., Burke, D., Patton, B. & Zurauskas, M. Aberrations and adaptive optics in super-resolution microscopy. *Microscopy (Oxf.)* **64**, 251–261 (2015).
54. Burke, D., Patton, B., Huang, F., Bewersdorf, J. & Booth, M.J. Adaptive optics correction of specimen-induced aberrations in single-molecule switching microscopy. *Optica* **2**, 177–185 (2015).
55. Huang, F. *et al.* Ultra-high resolution 3D imaging of whole cells. *Cell* **166**, 1028–1040 (2016).
56. Tehrani, K.F., Xu, J., Zhang, Y., Shen, P. & Kner, P. Adaptive optics stochastic optical reconstruction microscopy (AO-STORM) using a genetic algorithm. *Opt. Express* **23**, 13677–13692 (2015).
57. McGorty, R., Schnitzbauer, J., Zhang, W. & Huang, B. Correction of depth-dependent aberrations in 3D single-molecule localization and super-resolution microscopy. *Opt. Lett.* **39**, 275–278 (2014).
58. von Diezmann, A., Lee, M.Y., Lew, M.D. & Moerner, W.E. Correcting field-dependent aberrations with nanoscale accuracy in three-dimensional single-molecule localization microscopy. *Optica* **2**, 985–993 (2015).
59. Arigovindan, M., Sedat, J.W. & Agard, D.A. Effect of depth dependent spherical aberrations in 3D structured illumination microscopy. *Opt. Express* **20**, 6527–6541 (2012).
60. Thomas, B., Wolstenholme, A., Chaudhari, S.N., Kipreos, E.T. & Kner, P. Enhanced resolution through thick tissue with structured illumination and adaptive optics. *J. Biomed. Opt.* **20**, 26006 (2015).
61. Auksorius, E. *et al.* Stimulated emission depletion microscopy with a supercontinuum source and fluorescence lifetime imaging. *Opt. Lett.* **33**, 113–115 (2008).
62. Lenz, M.O. *et al.* 3-D stimulated emission depletion microscopy with programmable aberration correction. *J. Biophotonics* **7**, 29–36 (2014).
63. Gould, T.J., Burke, D., Bewersdorf, J. & Booth, M.J. Adaptive optics enables 3D STED microscopy in aberrating specimens. *Opt. Express* **20**, 20998–21009 (2012).
64. Mosk, A.P., Lagendijk, A., Lerosey, G. & Fink, M. Controlling waves in space and time for imaging and focusing in complex media. *Nat. Photonics* **6**, 283–292 (2012).
65. Horstmeyer, R., Ruan, H. & Yang, C. Guidestar-assisted wavefront-shaping methods for focusing light into biological tissue. *Nat. Photonics* **9**, 563–571 (2015).
66. Vellekoop, I.M. Feedback-based wavefront shaping. *Opt. Express* **23**, 12189–12206 (2015).
67. Sinefeld, D., Paudel, H.P., Ouzounov, D.G., Bifano, T.G. & Xu, C. Adaptive optics in multiphoton microscopy: comparison of two, three and four photon fluorescence. *Opt. Express* **23**, 31472–31483 (2015).
68. Jesacher, A. *et al.* Adaptive harmonic generation microscopy of mammalian embryos. *Opt. Lett.* **34**, 3154–3156 (2009).
69. Sun, W., Tan, Z., Mensh, B.D. & Ji, N. Thalamus provides layer 4 of primary visual cortex with orientation- and direction-tuned inputs. *Nat. Neurosci.* **19**, 308–315 (2016).